Evaluation of the Relative Permeability Hysteresis During the Alternating Injection of Brine and Nitrogen in Carbonate Rock using X-Ray Computed Tomography

Machado, C. G.[*], *Santos, R. G. dos*[†], *Bonet, E. J.*[‡], *Trevisan, O. V.*[§]

Department of Petroleum Engineering
State University of Campinas

Abstract

Water-alternating-gas (WAG) injection is an useful configuration for enhanced oil recovery (EOR). WAG consists in the improvement of the mobility control and areal sweep by cyclic injection of gas and water and it has been successfully applied worldwide. Application of WAG to carbonate reservoir has produced changes in the permeability curves during the injection cycles, which are assigned as permeability hysteresis. Consequently, hysteresis parameters obtained from experimental investigations are often required to adjust hysteresis models and to allow the improvement of the oil recovery prediction.

This work reports a laboratorial investigation on relative permeability hysteresis during alternating injection of high salinity brine and nitrogen into an oil saturated carbonate core under steady-state conditions. Main targets were to evaluate the permeability hysteresis and to assess the parameters to be applied in models of relative permeability hysteresis for numerical simulation.

Coquina core sample with porosity of 17% and 3.77 centimeters (diameter) by 20.24 centimeters (length) was obtained from an outcrop analog to the reservoir rocks of Brazilian Pre-salt. Sample was mounted inside an aluminum core-holder under a confinement pressure of 1,500 psi. Core was saturated with 200,000 ppm brine (50$\%wt\ NaCl$ and 50$\%wt\ NaI$) and next doped mineral oil ($18\,cP$ at $25\,^oC$) was injected to achieve the connate water saturation. Absolute permeability was obtained from the monophasic brine injection. Test were comprised by three injection cycles, starting from the imbibition curve (water-oil) followed two cycles of N_2/brine biphasic injections. Each cycle was performed in six different oil/brine and gas/brine ratios, in which the total flow was kept constant at $0.5\,cc/min$. X-Ray Computed Tomography (CT) was applied (130keV and 40 mA.s) to obtain a multiphasic quantitative analysis of the fluid in-situ saturations in the porous media.

Hysteresis effects on the relative permeability curves were observed in each cycle. Permeability hysteresis was mainly attributed to gas trapping in the porous media and to wettability changes during the injection cycles. In addition, the oil residual saturation was decreased along the successive cycles, achieving a 47% reduction. Brine-Nitrogen-Brine alternating injection results in a Land's constant at 0.93 and in an "*a*" parameter at 1.08. Since relative permeability data are essential parameters for reservoir engineering calculations, an important issue in WAG design was to obtain the hysteresis parameters to support simulation and prediction models.

Keywords: Hysteresis, relative permeability, immiscible WAG, Land constant, oil residual saturation factor

1 Introduction

Water-alternating-gas (WAG) injection is an useful configuration for enhanced oil recovery (EOR) and it has been successfully applied worldwide. Immiscible WAG consists in the improvement of oil recovery by raising the capillary number due to the

[*] cintiamachadorc@gmail.com
[†] ronaldo@cepetro.unicamp.br
[‡] bonet@dep.fem.unicamp.br
[§] trevisan@dep.fem.unicamp.br

relatively low interfacial tension between oil and gas and by the mobility control and areal sweep by the injection of water [Kulkarni, 2003]. Although WAG injection have been widely implemented, many uncertainties still hold on the fluid dynamic modeling that must be applied in reservoir simulation [Hosseini et al., 2012].

Results at WAG injection into carbonate rocks have shown changes in the permeability curves during the injection cycles, which is assigned as permeability hysteresis. Many authors have reported hysteresis effects in relative permeability experimental measurements. Eleri and Skauge [1995] have run tests in both steady and unsteady-state in carbonates. They found out that relative permeability curves, residual oil saturation and hysteresis effects differ on each method. In addition, Eleri and Skauge [1995] observed that hysteresis effects are more accentuated at transient methods, probably being consequence of fingers and preferential paths. Element et al. [2003] observed an increment in the oil recovery factor when WAG cycles are initiated by nitrogen injection during relative permeability measurements in intermediary to water-wet rocks. They also observed that residual water saturation after gas injection cycles are higher than critical water saturation in function of water trapping by gas and capillary effects in porous media. The last phenomenon was more expressive in strong water-wet rocks.

Hysteresis in relative permeability results from the saturation process (drainage and imbibition) and saturation history. It is related to the different wettability and fluid trapping [Spiteri and Juanes, 2006]. It is believed that hysteresis phenomenon is also connected with porous distribution and rock cementation [Honarpour et al., 1987]. Alteration of the rock wettability, and changes in capillary pressure curves are also known to have influence on relative permeability curves [Donaldson et al., 1989]. Several authors have investigated the impact of different relative permeability models applied to oil recovery prediction [Spiteri, 2005]. Spiteri and Juanes [2006] compared some models using experimental data. They concluded that water relative permeability curves does not show significant hysterisis effect in strong water-wet rocks and that the Land's coefficient may vary significantly according to the wetting behavior on dynamic conditions. They also observed that interpolation models generate distinct results and they usually overestimate gas relative permeability during WAG. Since the relative permeability of non-wetting fluid in triphasic system does not depend exclusively on its own saturation, it is not possible to estimate the relative permeability curves for these systems from conventional biphasic models [Larsen and Skauge, 1998].

Saturation history, wetting behavior, capillarity effects, porous geometry and its size distribution and many others petrophysical proprieties make the phenomenon of hysteresis in relative permeability a complex one. To take into account the global influence of these properties, two parameters have been included in relative permeability models. Residual oil saturation factor (a) parameter is obtained from W-G-W sucessive cycles, while the drainage reduction constant (α) parameter is obtaneid from G-W-G cycles. Larsen and Skauge's (1998) developed a cycle dependent numerical model that takes into account most of the features observed in WAG injection [Hosseini et al., 2012].

For a precise modeling of hysteresis, an experimental core analysis for each development project is necessary for identification of parameters to effectively study their effects on the process [Kulkarni, 2003]. However, according to Eleri and Skauge [1995], relative permeability curves can be obtained from synthetic fluids and outcrop rocks in atmospheric conditions, for the high costs and complexities of reproducing reservoir conditions and using real fluids and cores samples. Indeed, in consequence of experimental complexities and high costs, laboratorial data for multi-cyclic WAG is rarely found on the current literature [Hosseini et al., 2012].

Purpose. The two main purposes of this paper were the determination of the relative permeability curves during WAG injection in carbonates and the assessment of numerical parameters of relative permeability hysteresis for Larsen and Skauge's model (1998) to be used as input in simulation of reservoir production during immiscible WAG processes.

2 Experimental Apparatus and Procedures

X-Ray CT Scanner Description. The X-Ray CT tomography used is a Somaton X-ray CT (Siemens, German) medical scanner. The X-Ray source was used at 130 KeV energy level with 40 mA.s. Two milimeter equally spaced slices were made in each scan on the cores and CT completes a whole scan in 50 seconds. Although image (512x512 pixels reconstruction) resolution (0.1 mm) was not enough for porous visualization, it is sufficient to highlight medium heterogeneity. Figure 1 shows the image scan of the dry core.

For image processing, an algorithm was developed at software $MATLAB^{©}$7.10.0 (R2010a) using Image Processing Toolbox, after pre-processing at $OSIRIS^{©}$ 4.19, available as a general medical image manipulation and analysis software. An image processing routine to align the centre of core sections prior to CT subtraction was applied.

The dopant concentrations were determined after a graphical analysis of attenuation versus concentration in each liquid compared to nitrogen and rock attenuation in 130 keV energy level (Figure 2). Table 1 shows the CT numbers for fluids and for the rock completely saturated with each fluid used and at Figure 3 we can see its distribution along the core. For a damage occurred to the core sample, it was not possible to completely saturate the rock with oil after the test, so equation 19 was applied to estimate CTR_o.

No beam hardening effect was observed at image borders (CT numbers do not decrease towards the centre of the slice), as we can see in Figure 4, which presents the attenuation vertical distribution on dry, water saturated and oil at residual water saturated at the end section of the core.

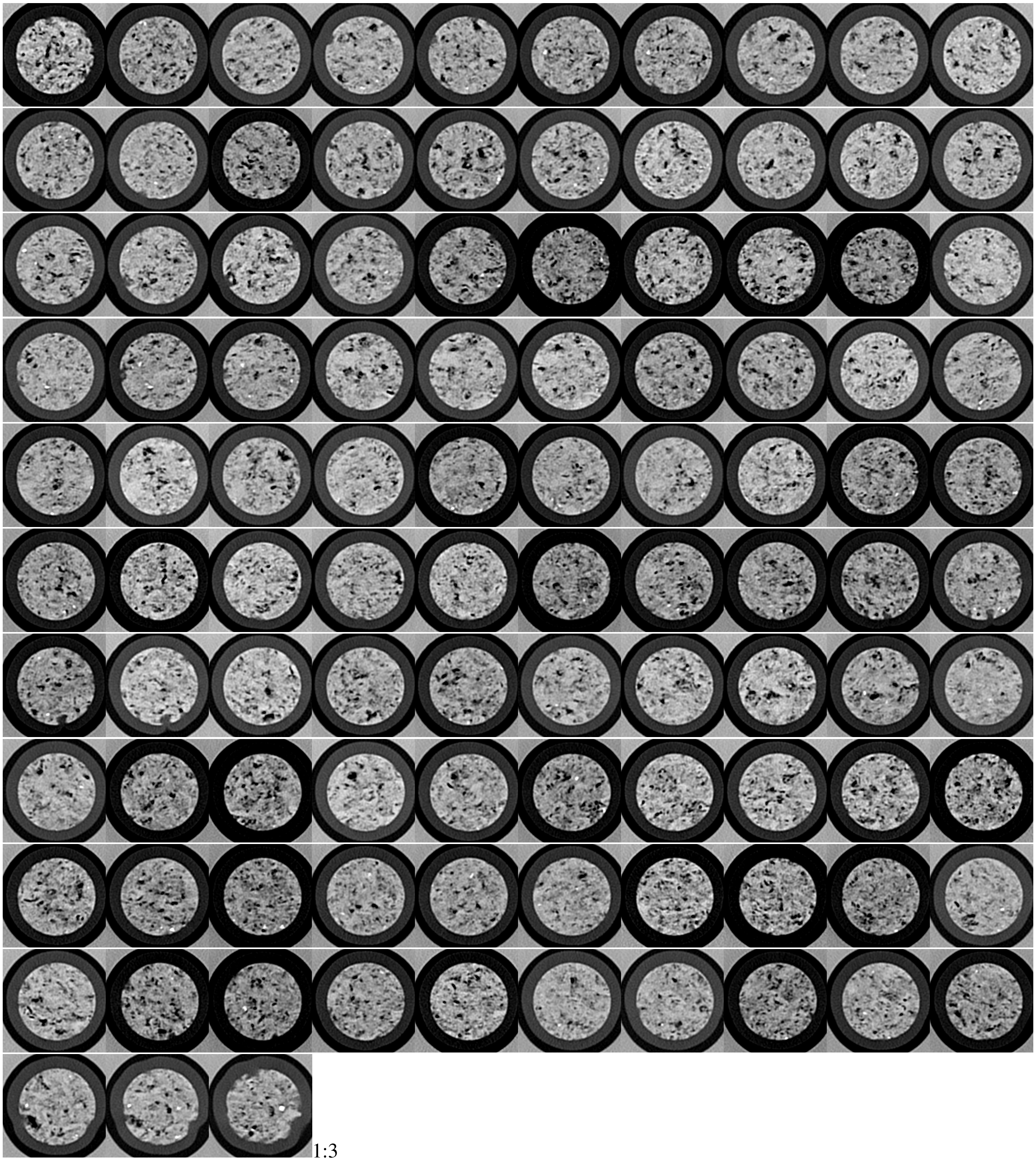

Fig. 1: X-Ray CT scan of dry core. The first slice was the end point of the core during dynamic flow testing.

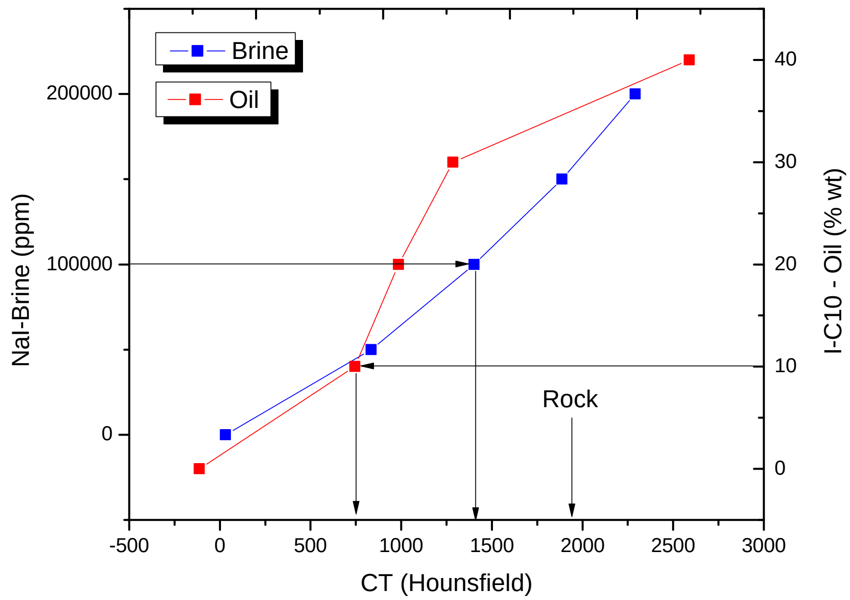

Fig. 2: Oil and brine attenuation according to dopants concentrations.

Tab. 1: CT numbers (130KeV).

Calcite Mineral	Brine	Oil	Gas	CTRn	CTRw	CTRo
1912	1572	745	-909	2894	3240	3125

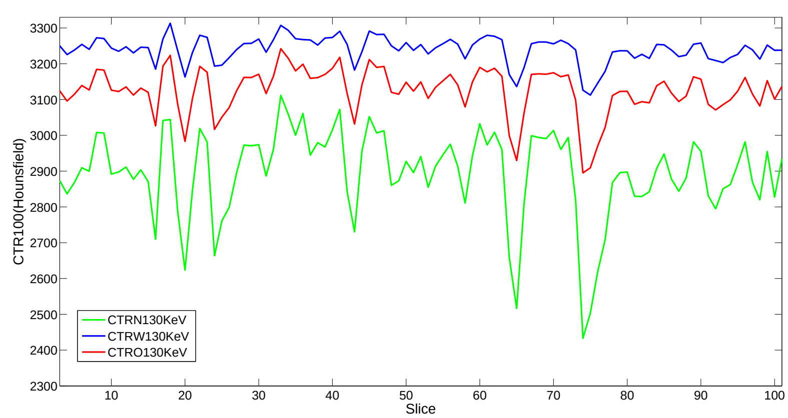

Fig. 3: Rock an hundred percent saturated attenuation for each fluid (nitrogen, oil and water).

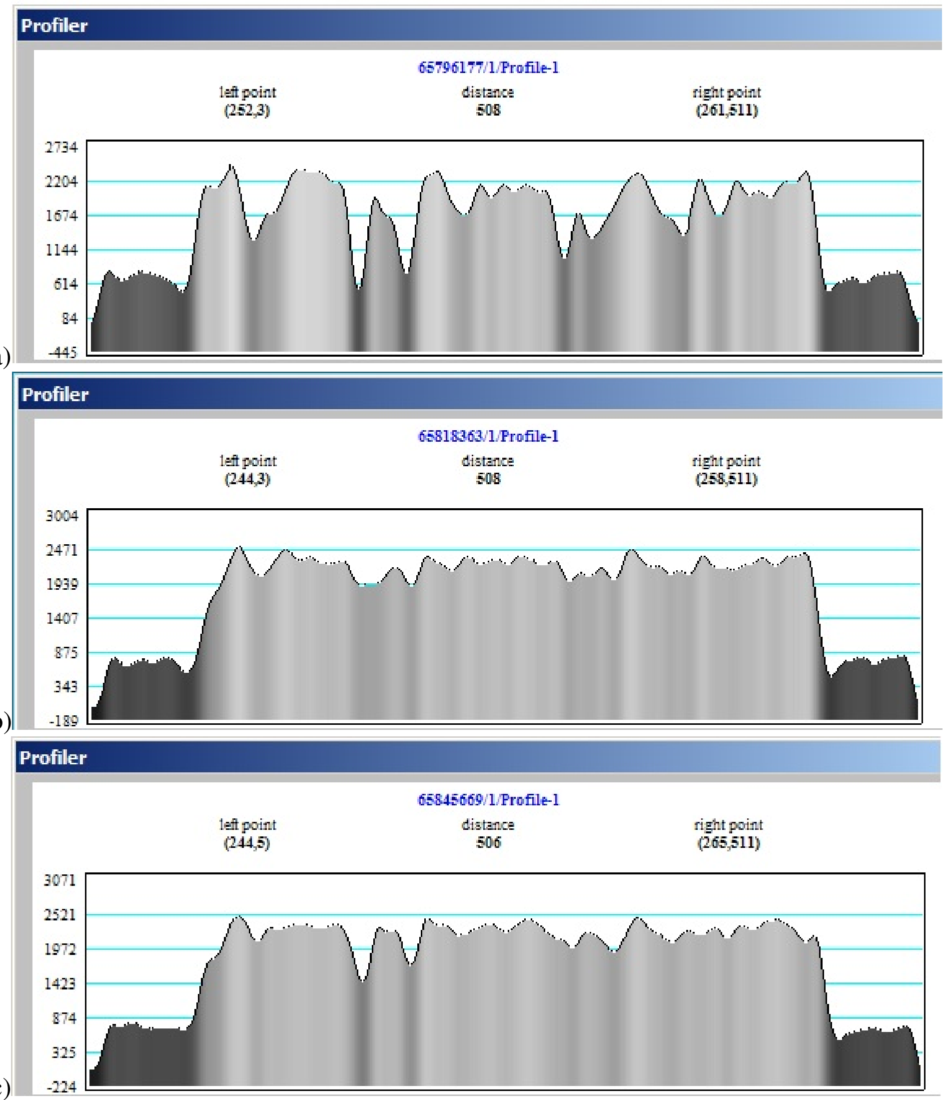

(a)
(b)
(c)

Fig. 4: CT distribution on dry (a), water saturated (b) and oil at residual water (c) saturated at end section of the core.

Core. A coquina core sample with 3.77 centimeters (diameter) by 20.24 centimeters (length) was obtained from an outcrop from Morro do Chaves Member, Coqueiro Seco Formation, Lower Cretaceous of the Sergipe-Alagoas Basin analog to reservoir rocks of Brazilian Pre-salt (Figure 5). Those coquina rocks are extremely heterogeneous [Dal'Bó, 2012] and according to Leon and Moreno [2012], their wettability is fractional to oil-wet.

1:3 1:1

Fig. 5: Coquina cores.

Core Cleaning and Core Installation. The outcrop core was cleaned by a sequential flow of methanol, toluene and dry nitrogen at room temperature (22ºC) and then dried at 80ºC for more than 72 hours.

After the cleaning and drying processes, cores were mounted inside an aluminum core-holder under a confinement pressure of 1,500 psi.

After the test, the core was cleaned by a sequential flow of toluene, methanol, toluene, methanol, hot dry nitrogen and then dried at 64ºC for more than 90 hours.

Fluids. The aqueous phase was composed of distillated, deionized and degassed high salinity brine (200,000 ppm), doped with NaI. The oil phase was deaired mineral oil (EMCA), doped with iododecane. Gas phase was humidified nitrogen. $NaCl$ was obtained from Chemco ($>$ 99.0%) and NaI from Sync ($>$ 99.0%). Physical Properties of all fluids used are given in Table 2. Fluid densities and apparent viscosities were measured with an Anton Paar DMA 4500 densimeter and a Haake Mars III rotating rheometer from Therma Scientific (Germany), using cone-plate geometry with titanium C60 tool (60 mm and 1^o) at 22^oC.

Tab. 2: Fluid Data at 22^oC.

	Brine (100,000 ppm NaCl/100,000 ppm NaI)	Mineral Oil (10%wt I-C10)	Nitrogen
Density (g/cm^3)	1.13828	0.87124	-
Viscosity (cP)	1.2	18.4	~0.018

Emulsion formation and salt precipitation tests were conducted in order to evaluate the interaction between the fluids. Both tests generated satisfactory results, as no emulsion or precipitation was observed.

Routine Core Analysis. The pore volume of the core was determined using an Ultra-pore 300 (CoreLab Instruments, USA) with N_2 and the absolute permeability with an Ultra-perm 500 (CoreLab Instruments, USA) with pure air before and after the test (Tables 3 and 4).

Tab. 3: Core Data before test.

Weight (g)	$Length$ (cm)	$Diameter$ (cm)	$Pore\ Volume$ (cm^3)	ϕ	ϕ $(X-RayCT)$	$k_{abs(gas)}$ (mD)	$k_{abs(brine)}$ (mD)	$k_{o@S_{wi}}$ (mD)
512.86	20.24	3.77	39.29	0.17	0.14	192	133	103

Tab. 4: Core data after test.

Weight (g)	Pore Volume End (cm^3)	ϕ	$k_{abs(gas)}$ (mD)
512.51	35.39	0.16	42

Saturation Procedures. The core was first of all saturated under vacuum with 200,000 ppm brine (50%$wt\,NaCl$ and 50%$wt\,NaI$). Absolute permeability was also obtained during the monophasic brine injection. Doped mineral oil (18 cP at 22 ^oC) was injected to achieve the initial water saturation.

Relative Permeability Tests. The relative permeability tests were conducted under steady-state conditions at room temperature (22$^o C$) (Figure 6).

Tests were comprised by three injection cycles, starting from the imbibition curve (water-oil) followed by two cycles of N_2/brine biphasic injections. Each cycle was performed at six different oil/ brine and gas/brine ratios, in which the total flow was kept constant at 0.5 cm3/min. In each condition were injected 10 to 20 porous volume (PV) in order to stabilize the flow, taking from several hours to days to achieve volumetric flow rate and pressure stability. X-Ray Computed Tomography (CT) was applied to obtain a multiphasic quantitative analysis of the fluid in-situ saturations in the porous media (Table 5).

Data acquisition. Pressure data from transducers and data of injected and produced fluid mass from digital balances were monitored and stored into the PC through *LabView*© software.

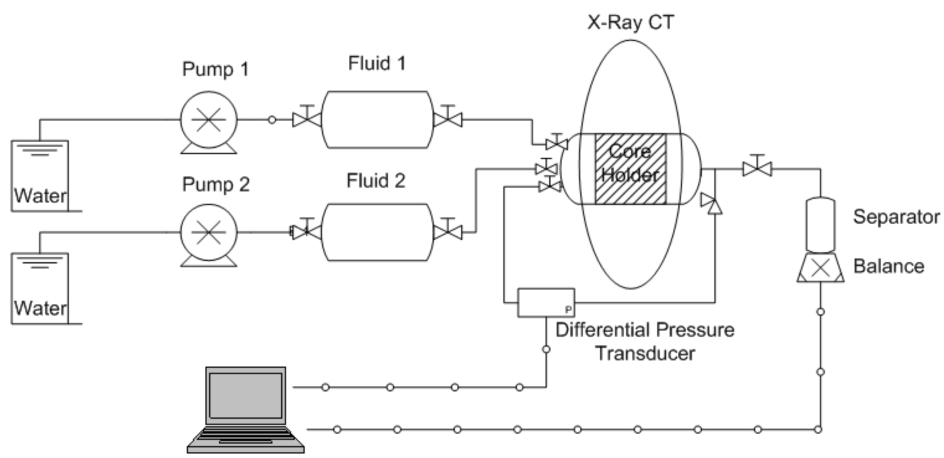

Fig. 6: Experimental Apparatus.

Tab. 5: Steady-state injection cycles.

Cycle	Description	Data Output
W	Water saturation	
O	Oil saturation	S_{oi}, S_{wi}
ID	Water (increasing) and Oil (decreasing) injection (1st Imbibiton)	S_{orow}, k_{rw}, k_{ro}
DDI	Water (decreasing) and Gas (increasing) injection (1st Drainage)	S_{gi}, k_{rw}, k_{rg}
IDD	Water (increasing) and Gas (decreasing) injection (2nd Imbibition)	S_{or}, S_{gt}, k_{rw}, k_{rg}

In this text, imbibition refers to increasing injection rate of water and drainage to increasing injection rate of oil or gas during the cycles, regardeless of the rock wettabillity.

3 Theoretical Approach

Relative Permeability. According to Honarpour et al. [1987], the relative permeability of a fluid is the ratio of the effective permeability of this fluid (k_r) to absolute permeability (k) of the rock or to oil effective permeability at initial water saturation ($k_{o@S_{wi}}$). The absolute permeability of a rock is its capability of allowing flow through itself. In the case of laminar flow, this propriety can by quantified by Darcy's Law (1856):

$$Q = \frac{kA}{\mu}\frac{\Delta P}{L}, \tag{1}$$

where Q is the volumetric rate and μ is the viscosity of fluid, A is the cross-sectional area, L is the length of the rock and $\triangle P$ is the pressure drop along the flow. If there is more than one fluid in a porous media, equation 1 can be modified with the effective permeability concept, which states that the conductivity of each fluid depends on its own saturation in the medium (fluid volume/void-space volume), rock wettability and porous distribution for a liquid phase [Amyx et al., 1960]:

$$Q_{phase} = \frac{k_{effective\, phase}A}{\mu_{phase}}\frac{\Delta P}{L} \tag{2}$$

and for a ideal gas phase [Rosa et al., 2006]:

$$Q_g(x) = \frac{k_{effective\, g}A}{\mu_{phase}}\frac{\Delta P}{L}\frac{(P_{inlet}+P_{outlet})}{2P(x)}. \tag{3}$$

Usually, relative permeability curves are constructed by relating relative permeabilities with wetting fluid saturation. When gas is present in the system, total liquid saturation is applied, as the gas is always the non-wetting fluid. Water fractionary flow (f_w) can be obtained from Darcy equation:

$$f_w = \frac{Q_w}{Q_{total}}, \tag{4}$$

where $Q_{total} = \sum Q_{phase}$.

Steady-State Determination of Relative Permeability Curves. If more than two fluids flow through the porous media, relative permeabilities curves for each fluid may be obtained by means of interpolation of curves of relative permeability drawn in biphasic experimental tests instead of running high cost and time-consuming triphasic experiments [Spiteri, 2005]. Relative permeability curves for biphasic system can be determinated by either steady-state or unsteady-state methods. Although transient methods are much less time-consuming, they are quite complex and dependent on restrictions related to the mobility ratio and the capillary number, preveting finger formation and piston-like flow. If these conditions are not achieved, which usually happens in heterogeneous medium, the data accuracy probably will be out of acceptation [Schembre and Kovscek, 2003]. On the other hand, steady-state methods yield relative permeability directly from Darcy's Law in different equilibrium points by varying water fractional flow.

Relative permeability curves generated from experimental data can be correlated through Corey equation [Standing, 1974]. For biphasic flow, water relative permeability (k_{rw}^{Imb1}) and oil relative permeability (k_{ro}^{Imb1}) are function of dimensionless water saturation (S_{wD}):

$$k_{rw}^{Imb1} = k_{rw@S_{orow}}(S_{wD})^{nm^{Imb1}} \tag{5}$$

and

$$k_{ro}^{Imb1} = k_{ro@S_{wi}}(1-S_{wD})^{m^{Imb1}}, \tag{6}$$

$$S_{wD} = \frac{S_w - S_{wi}}{1 - S_{orow} - S_{wi}}, \tag{7}$$

where the superscript $Imb1$ represents 1^{st} Imbibition cycle, S_{orow} is residual oil saturation after waterflood and S_{wi}, initial water saturation. Whereas nm and m are Corey indices. For 1^{st} drainage cycle, in a triphasic flow, water relative permeability (k_{rw}^{Drain}) and gas relative permeability (k_{rg}^{Drain}) can be related to dimensionless liquid saturation (S_{LD}):

$$k_{rw}^{Imb2} = k_{rw@S_{sorow}} (S_{LD}^{Drain})^{nm^{Drain}}. \tag{8}$$

$$k_{rg}^{Drain} = k_{rg@S_{gi}} (1 - S_{LD}^{Drain})^{m^{Drain}}, \tag{9}$$

and

$$S_{LD}^{Drain} = \frac{S_L - S_{orDrain} - S_{wrDrain}}{1 - S_{orDrain} - S_{wrDrain}}, \tag{10}$$

where the superscript $Drain$ represents 1^{st} drainage cycle. $S_{orDrain}$ and $S_{wrDrain}$ are residual oil and residual water saturation after drainage, respectively. Finally, for 2^{nd} imbibiton cycle, water relative permeability (k_{rw}^{Imb2}) and gas relative permeability (k_{rg}^{Imb2}) can be also related to dimensioless liquid saturation:

$$k_{rw}^{Imb2} = k_{rw@S_{gt}} (S_{LD}^{Imb2})^{nm^{Imb2}}, \tag{11}$$

$$k_{rg}^{Imb2} = k_{rg@S_{gi}} (1 - S_{LD}^{Imb2})^{m^{Imb2}}, \tag{12}$$

and

$$S_{LD}^{Imb2} = \frac{S_{LD} - S_{or}}{1 - S_{or} - S_{gt}}, \tag{13}$$

where the superscript $Imb2$ represents 2^{nd} imbibition cycle. S_{or} is residual oil saturation and S_{gt} is trapped gas saturation, after this cycle.

Numerical Hysteresis Parameters. In a WAG recovery process, both oil saturation and relative permeabilities are reduced during injection cycles. This occurs in function of the fluid trapping in porous media, which has an important role in residual oil mobilization [Sanchez, 1999]. Characterization of the fluid trapping phenomenon is necessary for permeability curves behavior prediction. Experimental data suggests that there are not significant hysteresis effects in the wetting phase. There is a sort of empiric models for non-wetting phase relative permeability and saturation under hysteresis effects available[Spiteri, 2005]. Modeling of the hysteresis effects are based in two extreme curves related to saturation process with a set of intermediary curves between them. The first one is irreversible and the latest is reversible [Braun and Hollan, 1995].

Land [1971] proposed an empirical constant based on experimental data obtained from drainage after an imbibition process in order to calculate trapped gas saturation:

$$C = \frac{1}{S_{gt}} - \frac{1}{S_{gi}}, \tag{14}$$

where C is the Land's constant and S_{gi} is maximum gas saturation. Most of the hysteresis models are based in this empiric trapping model proposed by Land, which was developed from water-wet sandstone experimental data. Land‘s constant is a function of the interfacial tension between fluids and medium permeability and it is not constant during cyclic water/gas injection [Spiteri, 2005].

As in a triphasic system the relative permeabilities of non-wetting fluids are dependent not only of their saturations, it is not possible to estimate these curves from conventional biphasic models. Larsen and Skauge[Larsen and Skauge, 1998] developed intermediary curves for relative permeability during imbibition and drainage processes. They defined an empirical relationship between three-phase residual oil saturation (S_{or}), residual oil saturation after waterflood and trapped gas saturation as:

$$S_{or} = S_{orow} - aS_{gt}. \tag{15}$$

Larsen and Skauge [1998] demonstrated how to use those parameters, in addtion with gas-oil relative permeabilities curves and drainage reduction constant that are out of the scope of this paper, to generate cyclic relative permeability curves having hysteresis effects in WAG recovery process.

Porosity and In-situ Saturation X-Ray Measurements. In order to generate relative permeability curves, fluid saturations could come not only from material balance, but also from in situ weighting, resistivity logs, nuclear magnetic resonance and X-Ray absorption, among others [Honarpour et al., 1987]. In comparison to those techniques, CT X-Ray measurement of saturation is fast, accurate, easy to calibrate and offers fine spatial resolution [Mees et al., 2003]. CT X-Ray imaging techniques allow the visualization of porosity and fluid distribution inside the porous media. Core porosity (ϕ) can be obtained from X-Ray scan based in the fact that attenuation contribution from matrix rock and from fluids saturating it are independent [de Holleben, 1993]:

$$\phi = \frac{CTR_w - CTR_n}{CT_w - CT_n}, \tag{16}$$

derived from the follow system:

$$\begin{cases} (1-\phi)CT_{RockMatrix} + \phi CT_n = CTR_n \\ (1-\phi)CT_{RockMatrix} + \phi CT_w = CTR_w, \end{cases} \tag{17}$$

where CT is the computed tomography number (HOUNSFIELD units):

$$CT = 1000(\frac{\psi}{\psi_w} - 1), \tag{18}$$

ψ is the attenuation linear coefficient and CTR are the CT number for the core saturated with fluids. Whereas, the subscripts w and n represents water and nitrogen phase, respectively.

If it is not possible to obtain the rock completely saturated with oil, the following correlation (Figure 7) can be used:

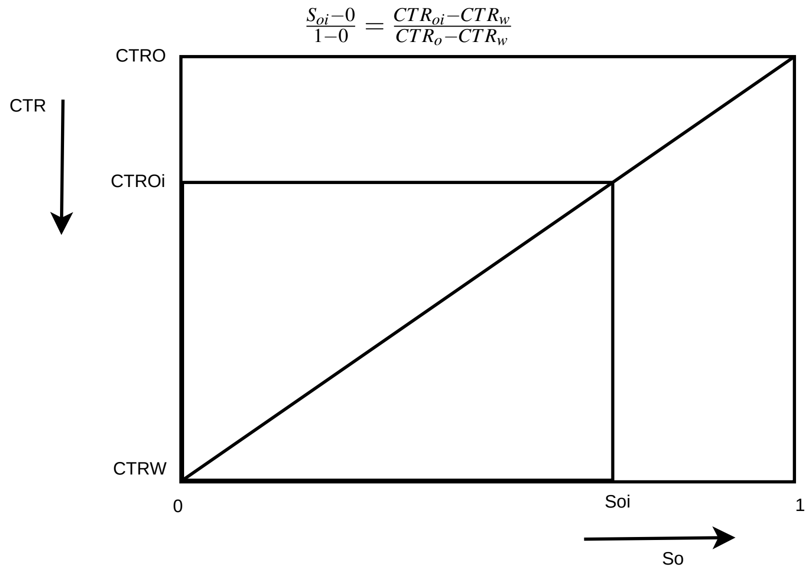

Fig. 7: Linear relantionship between CTR and oil saturation. Adaptation from Holleben (1993).

$$CT_{Ro} = \frac{CT_{Roi} - CT_{Rw}}{S_{oi}} + CT_{Rw}, \tag{19}$$

proposed by Wellington and Vinegar [1987], where initial oil saturation (S_{oi}) distribution along of the core is obtained from equation 20:

$$S_{oi} = \frac{(CTR_w - CTR_{oi})}{\phi(CT_w - CT_o)} \tag{20}$$

and

$$S_{wi} = 1 - S_{oi}, \tag{21}$$

derived from the follow system:

$$\begin{cases} (1-\phi)CT_{RockMatrix} + \phi CT_w = CTR_w \\ (1-\phi)CT_{RockMatrix} + \phi(S_{wi}CT_w + S_{oi}CT_o) = CTR_{oi} \\ S_{oi} + S_{wi} = 1, \end{cases} \tag{22}$$

where S_{oi} is initial oil saturarion. CTR_{oi} represents core CT number at initial condition. In this metodology, it is introduced the hypothesis that fluids attenuation is the same inside and outside of porous medium [de Holleben, 1993].

For in-situ saturation measurements, for both biphasic and triphasic process, it can be used a linear regression, cited in Mees et al. [2003], which consider that a linear relationship between fluid saturation and system X-Ray attenuation holds. For first imbibition cycle, in this technique, it is assumed that the CT number of the core lies on the straight line connecting rock completely saturatated by oil to brine phase (Figure 10):

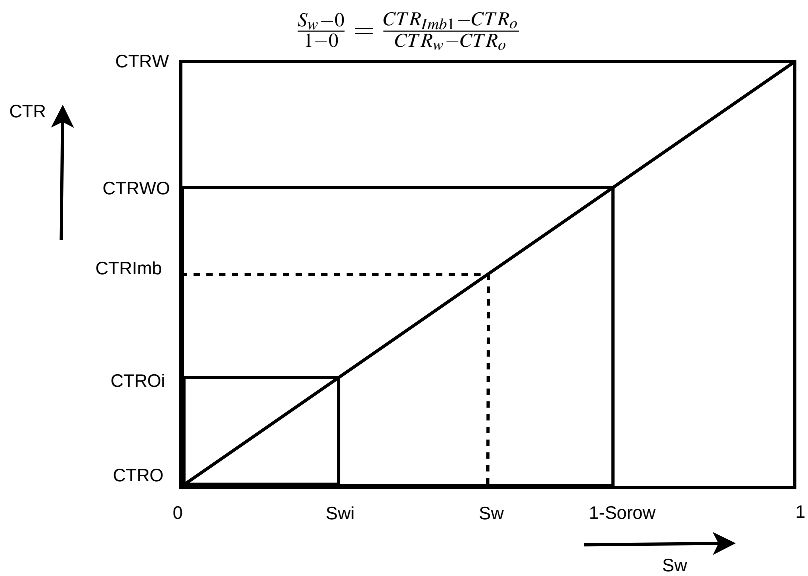

Fig. 8: 1^{st} Imbibition.

$$Sw = \frac{CTR_{Imb1} - CTR_o}{CTR_w - CTR_o} \tag{23}$$

and

$$S_o = 1 - S_w, \tag{24}$$

where the subscripts $Imb1$ represents the CT numbers from 1^{st} imbibition cycle. For first drainage cycle, it is assumed that the CT number of the core lies on the straight line connecting rock saturated by water-oil at end point of 1^{st}imbibition cycle to rock completely saturatated by nitrogen phase (Figure 9):

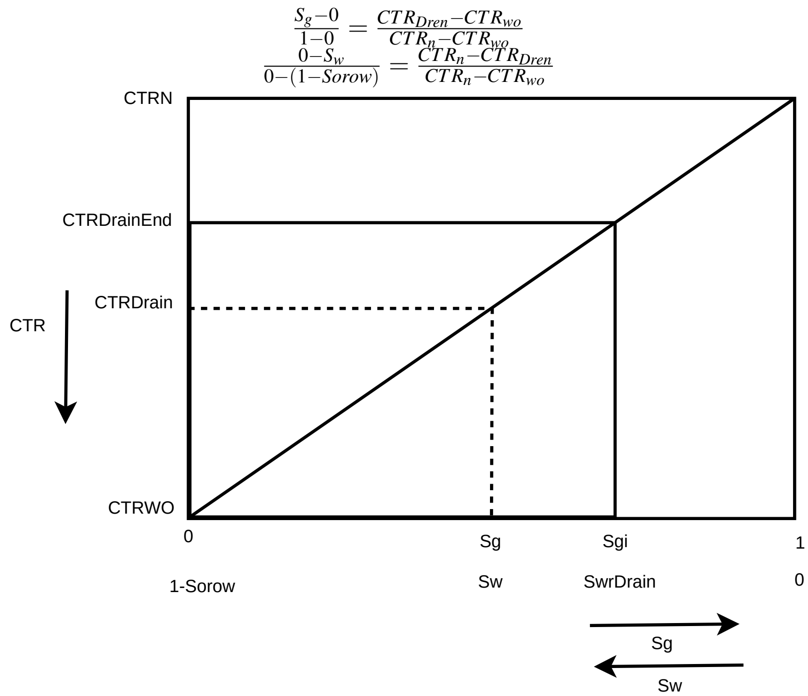

Fig. 9: 1st Drainage.

$$S_w = (1 - S_{orow}) \left(\frac{CTR_n - CTR_{Drain}}{CTR_n - CTR_{wo}} \right), \tag{25}$$

$$S_g = \frac{CTR_{Drain} - CTR_{wo}}{CTR_n - CTR_{wo}} \tag{26}$$

and

$$S_{or} = 1 - S_w - S_g, \tag{27}$$

where the subscripts *Drain* represents CT numbers from 1st drainage cycle and *wo*, the end point of 1st imbibition cycle. For second imbibition cycle, it is assumed that the CT number of the core lies on the straight line connecting rock saturated by water-gas-oil at end point of 1st drainage cycle to rock completely saturatated by brine phase (Figure 10):

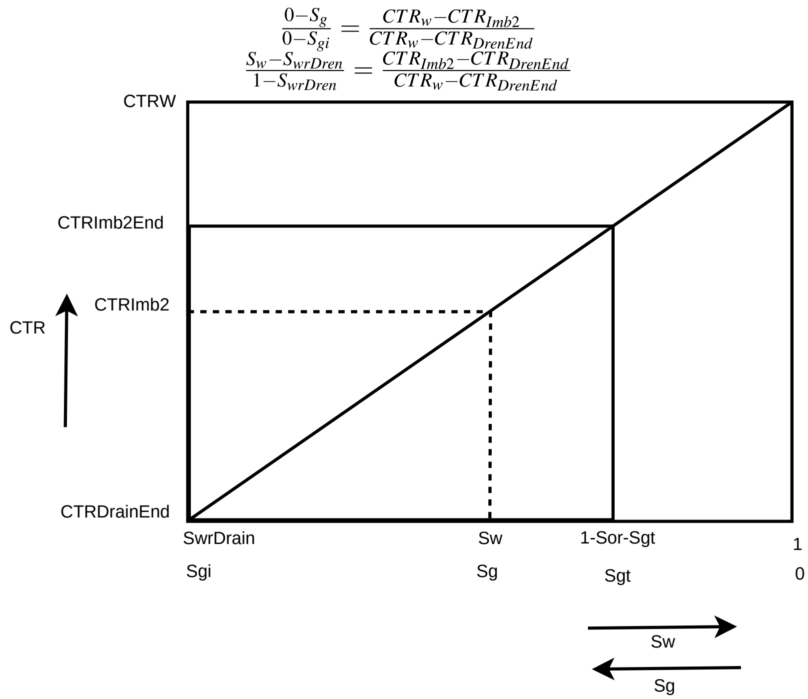

Fig. 10: 2^{nd} Imbibition.

$$S_w = (1 - S_{wrDrain}) \left(\frac{CTR_{Imb2} - CTR_{DrainEnd}}{CTR_w - CTR_{DrainEnd}} \right) + S_{wrDrain}, \tag{28}$$

$$S_g = (S_{gi}) \left(\frac{CTR_w - CTR_{Imb2}}{CTR_w - CTR_{DrainEnd}} \right) \tag{29}$$

and

$$S_{or} = 1 - S_w - S_g, \tag{30}$$

where the subscripts $Imb2$ represents CT numbers from 2^{nd} imbibition cycle and $DrainEnd$, the end point of 1^{st} drainage cycle. Whereas, $S_{wrDrain}$ is residual water saturation at end point of 1^{st} drainage cycle. This experimental procedure is somewhat less complicated than dual-energy techniques for triphasic saturation measuraments, because the optimal dopant concentrations in each phase calibration are needed at just one energy level. In addition, experimental costs related to CT X-Ray use are minimized.

4 Results and Discussions

Porosity distribution along the core is presented at Figure 11, which confirms the porous media heterogeneity, with a porosity value varying from 8% to 28%. Figures 12, 13 and 14 show fluid saturation distribution along the core in each equilibrium point of steady-state relative permeability test for each injection cycle (flow direction is from right to left). It was observed a water accumulation in the beginning of the core at the end of second imbibition cycle, which persists after 20 PV injected. This phenomenon remains unknown and under investigation.

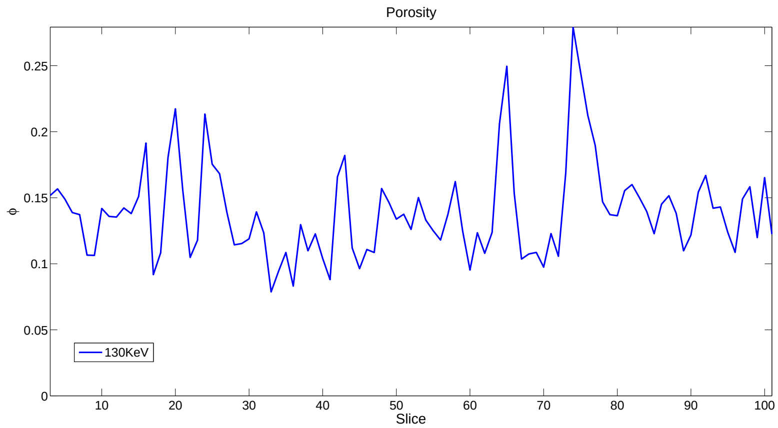

Fig. 11: Porosity Distribution along the core.

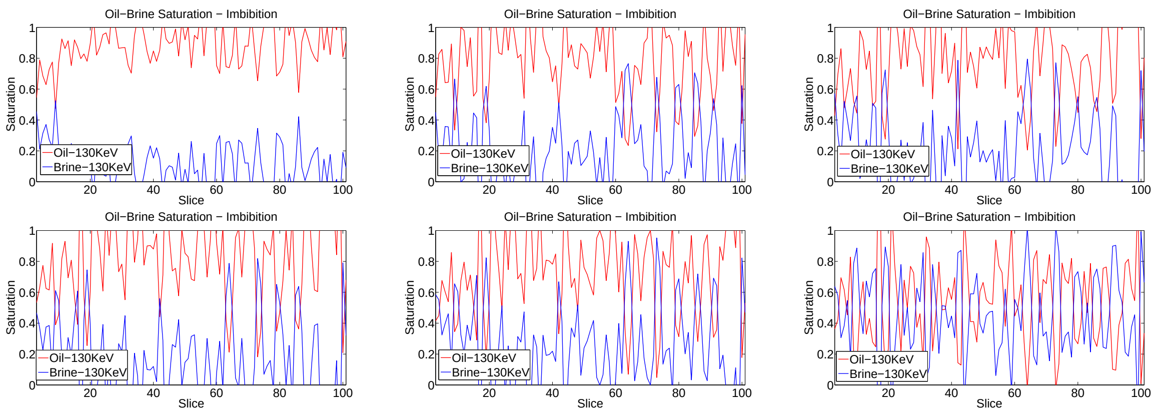

Fig. 12: Saturations distribution along the core (1^{st} Imbibition) for each point of equilibrium. Flow direction is from slice 101 (right) to 1 (left).

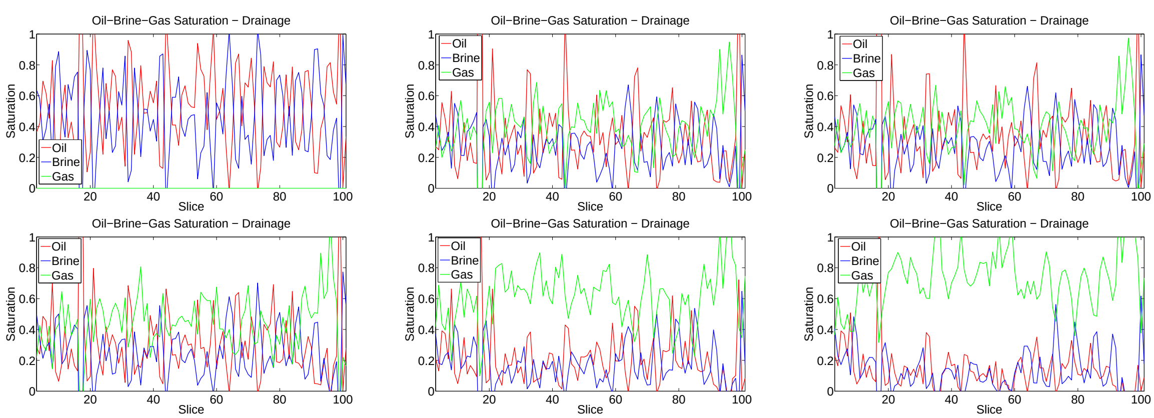

Fig. 13: Saturations distribution along the core (1^{st} Drainage) for each point of equilibrium. Flow direction is from slice 101 (right) to 1 (left).

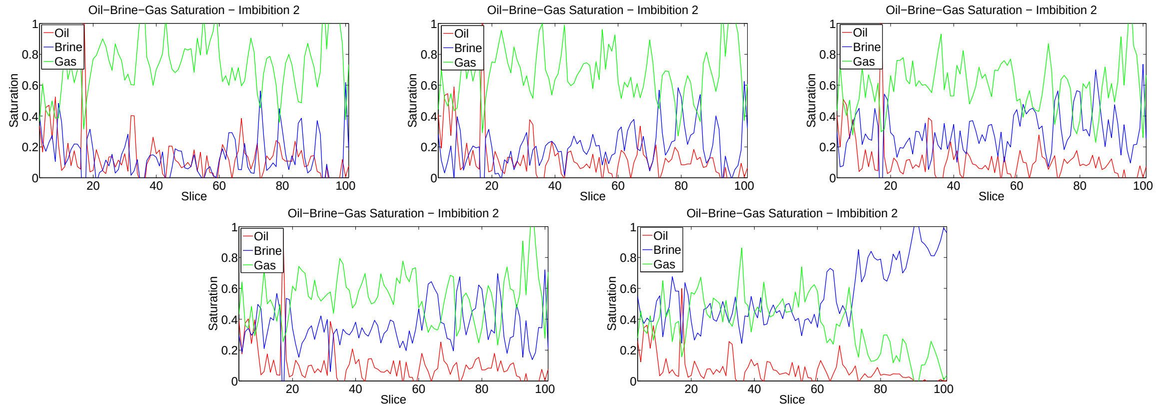

Fig. 14: Saturation distribution along the core (2^{nd} Imbibition) for each point of equilibrium. Flow direction is from slice 101 (right) to 1 (left).

Figure 15 shows the path of three-phase saturation during immiscible WAG injection. Initial oil saturation and residual oil saturation after waterflooding were significantly high, 88% and 54%, respectively. According to Amyx et al. [1960], the critical saturation for non-wetting fluid usually varies between 0 to 15%. These data can be correlated with a possible fractional wettability to oil wet behavior of the rock, as those coquina cores were characterized by Leon and Moreno [2012]. Water residual saturation (*Swr*) after gas injection cycle was higher, albeit slightly (just 1%), than initial water saturation (*Swi*), in agreement with water trapping by gas description done by Element et al. [2003]. Besides, the maximum water saturarion (end point of 2^{nd} imbibition cycle) was 10% higher than water saturation at oil-water imbibition cycle end point. According to Spiteri and Juanes [2006], this is a common behavior for most EOR systems. In addition, a 37% of gas was trapped after second imbibition and the oil residual saturation was decreased along the successive cycles, achieving a 47% reduction. Average oil residual saturation factor measured was 1.27 and average Land's constant measured was 1.35 (Table 6). Figures 16 and 17 show those parameters, *a* and *C*, distribution along the core. It is evident the influence of the water accumulation cited. If we take in account only the last 70 images (Figures 18 and 19), a and C core parameter would be 1.08 and 0.93, respectively.

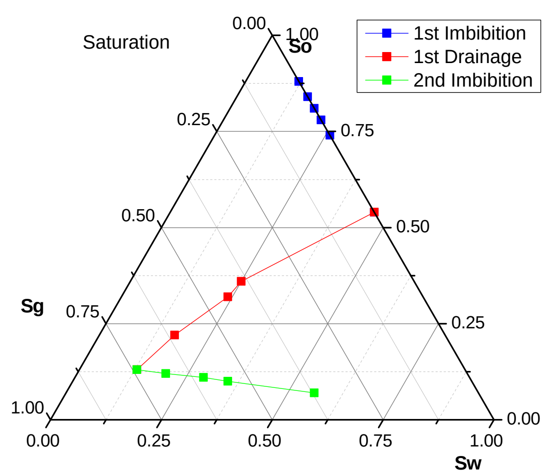

Fig. 15: Saturation Ternary Diagram.

Tab. 6: Experimental parameters results from WAG test.

	Initial	End 1^{st} Imbibition	End 1^{st} Drainage	End 2^{nd} Imbibition	a	C
S_o	0.88	0.54	0.13	0.07	1.08	0.93
S_w	0.12	0.46	0.13	0.56		
S_g	0	0	0.74	0.37		

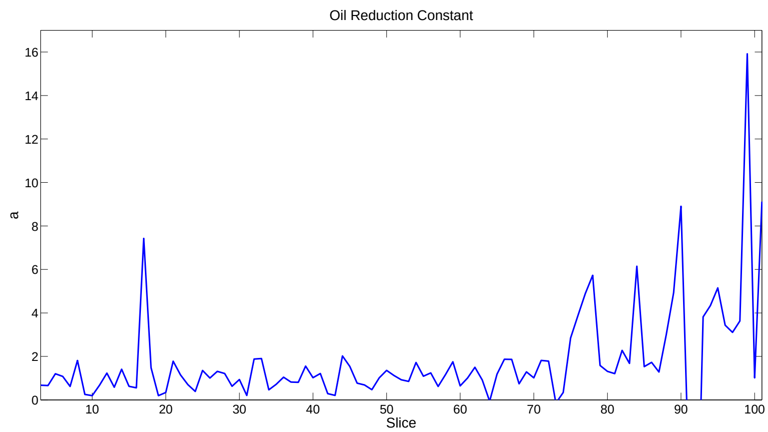

Fig. 16: Residual oil saturation factor along the core.

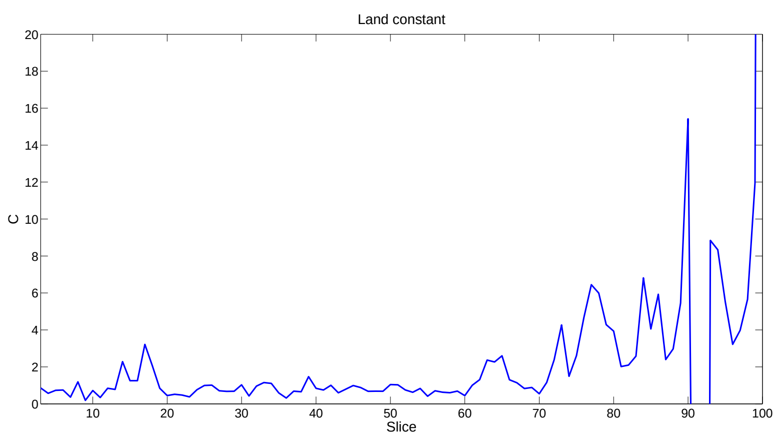

Fig. 17: Land‘s constant along the core.

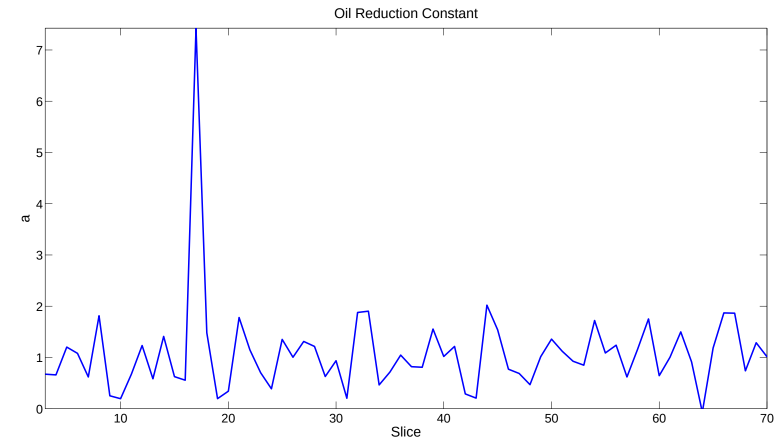

Fig. 18: Residual oil saturation factor along the last 14 cm of the core.

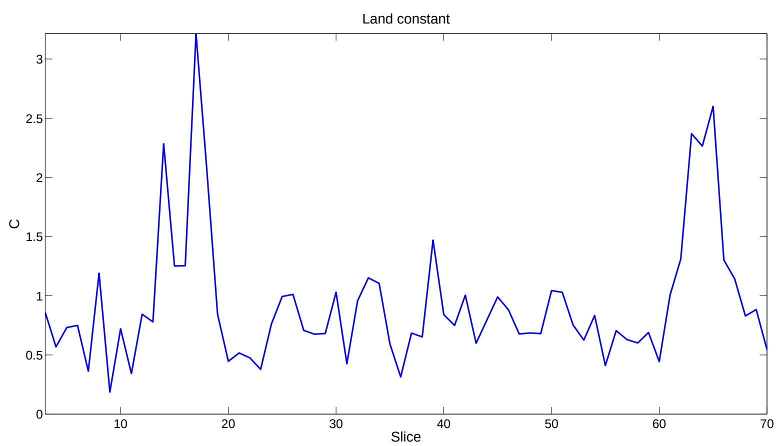

Fig. 19: Land's constant along the the last 14 cm of the core.

Test was initiated at $1\,cm^3/min$. However, the injection pressure tended quickly to the limit of the overburden pressure imposed at the core-holder ($1500\,psi$) at the 4^{th} point of first imbibition cycle. Then the flow rate was changed to $0.5\,cm^3/min$. Tables 7, 8 and 9 are presentes the experimental data obtained on first imbibition, first drainage and second imbibition, respectively. Relative permeability data and water fractional flow were fitted with Corey equation (Figures 20, 21, 22). Curves were better fitted by using an "homogenous" indices for water curves and "heterogeneous" indices for oil and gas curves (Table 10), instead of the usual procedure applied to Corey equation. This fact is supposed to be resulting from fractional wettability characteristic of this core. It is thought that each fluid flow according to porous size and their wettablility. Probably, the smaller and more homogenous porous tends to a water-wettability behavior while the bigger and more heterogeneous porous tends to an oil-wettability behavior. However, there is no currently data available to support this supposition.

Tab. 7: Experimental data from 1^{st} Imbibition.

$q_w\,(cm^3/min)$	$q_o\,(cm^3/min)$	$\triangle p\,(psi)$	k_{rw}	k_{ro}	S_w	S_o
0	1	79	0	0.7764	0.12	0.88
0.02	0.98	139	0.0006	0.4324	0.22	0.78
0.1	0.9	399	0.0010	0.1383	0.19	0.81
0.125	0.375	725	0.0007	0.0317	0.16	0.84
0.375	0.125	687	0.0022	0.0112	0.26	0.74
0.5	0	360	0.0056	0	0.46	0.54

Tab. 8: Experimental data from 1^{st} Drainage.

$q_w\,(cm^3/min)$	$q_g\,(cm^3/min)$	$\triangle p\,(psi)$	k_{rw}	k_{rg}	S_w	S_g	S_{or}
0.5	0	360	0.0056	0	0.46	0	0.54
0.35	0.15	531	0.0026	0.00003	0.25	0.39	0.36
0.3	0.2	530	0.0023	0.00005	0.25	0.39	0.36
0.2	0.3	461	0.0017	0.0001	0.24	0.44	0.32
0.01	0.49	166	0.0002	0.0004	0.17	0.61	0.22
0	0.5	35	0	0.0017	0.13	0.74	0.13

Tab. 9: Experimental data from 2^{nd} Imbibition.

$q_w\,(cm^3/min)$	$q_g\,(cm^3/min)$	$\triangle p\,(psi)$	k_{rw}	k_{rg}	S_w	S_g	S_{or}
0	0.5	35	0	0.0017	0.13	0.74	0.13
0.01	0.49	211	0.0004	0.0005	0.20	0.68	0.12
0.05	0.45	113	0.0009	0.0002	0.29	0.60	0.11
0.15	0.35	373	0.0016	0.0001	0.35	0.55	0.10
0.5	0	509	0.0039	0	0.56	0.37	0.07

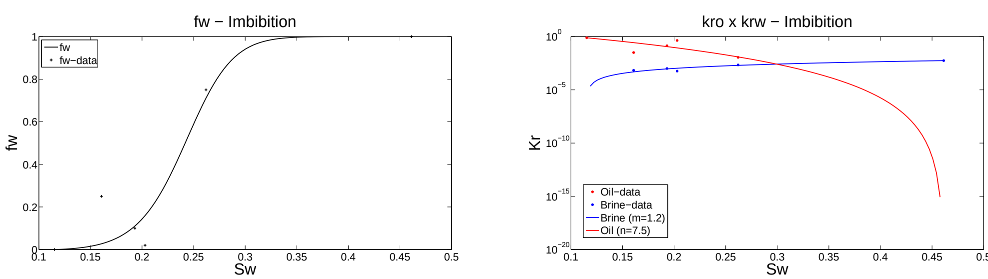

Fig. 20: Fractional flow and relative permeability curves (ID).

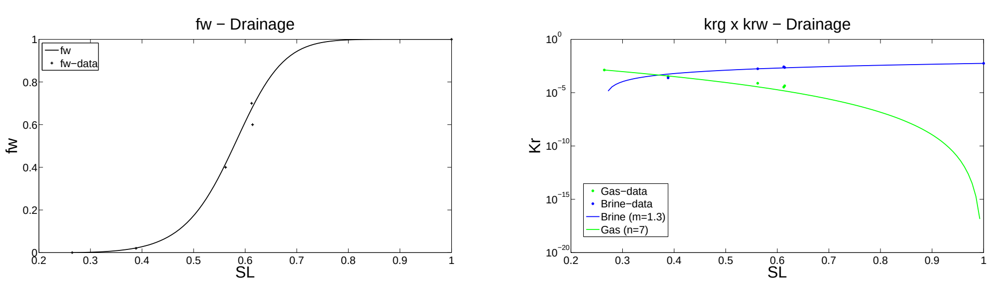

Fig. 21: Fractional flow and relative permeability curves (DDI).

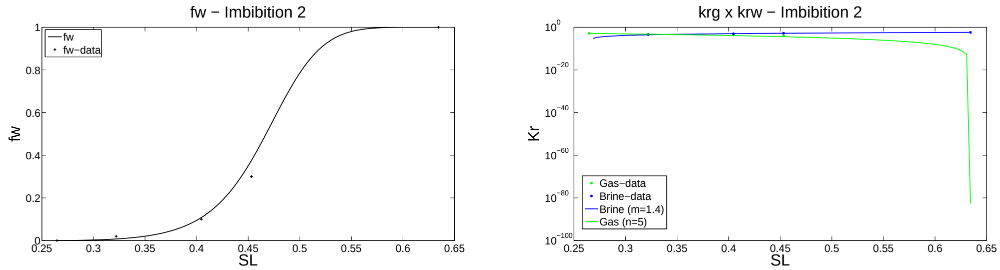

Fig. 22: Fractional flow and relative permeability curves (IDD).

Tab. 10: Relative permeability curves fititing.

	1^{st} Imbibition	1^{st}Drainage	2^{nd}Imbibition
nm	1.2	1.3	1.4
m	7.5	7	5

Alternating injection of immiscible fluids have promoted alterations on phase saturation and consequently on relative permeability curves. Figure 23 shows the evolution of gas relative permeability and Figure 24 shows the evolution of water relative permeability during immiscible WAG injection. Hysteresis effects in those curves are clearly observed through the decreasing in relative permeability values cycle by cycle. Permeability hysteresis was attributed to gas trapping in the porous media during the injection cycles. Besides hysteresis effects, unusual very low water relative permeability values were measured. This may be explained by a core damage suffered during the test, which was reflected in a 1% decreasing in porosity and a 78% in absolute permeability data. It is thought that this damage was caused by salt precipitation and fine migration, ascribed to water-sensitivity phenomenon. The salt precipitation would be a consequence of the fluactuation of pressure inside the porous as well as of the mass transfer between brine and nitrogen. Rock damage during relative permeability tests in carbonates was cited in Withjack and Duham as a recurrent problem. Besides, Lopes and Moreno [2012] have found water relative permeability values of the same order of magnitude for those coquina rock in an brine-mineral oil system. However, as they did not report absolute permeability and porosity data after testing, it was not possible to compare if some kind of rock damage have ocurred.

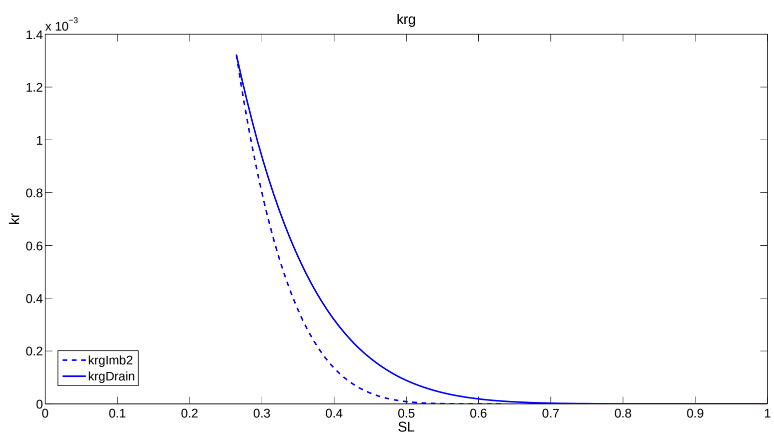

Fig. 23: Comparation between gas relative permeability curves.

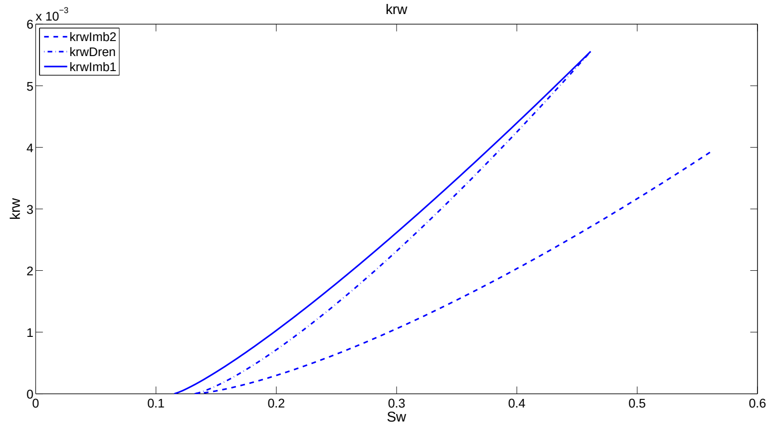

Fig. 24: Comparation between water relative permeability curves.

5 Conclusions

- Porosity data obtained from X-Ray CT confirms porous media heterogeneity, with a porosity value varying in 20% along the core.
- Fluid saturation distribution along the core shows a water accumulation in the beginning of the core at the end of second imbibition cycle, which persists after 20 PV injected. This phenomenon remains unknown and under investigation, since it has significant influence on Larsen and Skauge parameters measured.
- Alternating injection of immiscible fluids have been pointed out to promote alterations on phase saturation and consequently on relative permeability curves. Initial oil saturation and residual oil saturation after waterflooding were significant high, decreasing along the successive cycles, and achieving 47% total reduction. Initial water saturation was less than 15% and water residual saturation after gas injection cycle was slightly higher than the initial water saturation. These data corroborate that this sample is not strong water wet. In addition, a high volume (almost 40%) of gas was trapped after second imbibition.
- Relative permeability data were fitted with Corey equation. Corey indices for homogenous media were applied for water relative permeability curves and indices for heterogeneous porous media were applied for oil and gas relative permeability curves. These results may be related to flow behavior in a fractional wet rock, where the smaller and more homogenous porous could show a water-wettability tendency.
- Relative permeability hysteresis was observed in both water and gas curves. Permeability hysteresis was attributed to gas trapping in the porous media during the injection cycles. Besides, it was detected a damage on the core during the experiment, which was related with fine migration and salt precipitation, contributing to very low water relative permeability values.

6 Acknowledgements

Authors gratefully thank to PRH-ANP/PETROBRAS studentship and to the financial support from PETROBRAS S.A.

7 Nomenclature

S_o	=	Oil saturation
S_w	=	Water Saturation
S_g	=	Gas saturation
S_{wi}	=	Irreducible Water Saturation
S_{or}	=	Three-phase residual oil saturation
S_{orow}	=	Residual oil saturation after waterflood
S_{gi}	=	Maximum historical gas saturation
S_{gt}	=	Trapped gas saturation
S_L	=	Liquid Saturation
C	=	Land's Constant
a	=	Residual oil saturation factor
α	=	Drainage reduction constant
k_{ro}	=	Oil relative permeability
k_{rw}	=	Water relative permeability
k_{rw}	=	Gas relative permeability
μ	=	Viscosity (cp)
ρ	=	Density ($\frac{g}{cm^3}$)
ϕ	=	Porosity
ψ	=	Attenuation linear coefficient
CT	=	Computed tomography number (Hounsfield)
CTR_f	=	CT number of rock completely saturated with fluid f
CT_f	=	CT number of fluid f ($HOUNSFIELD$)
L	=	Core lenght (cm)
A	=	Tranversal Area (cm^2)
ΔP	=	Pressure drop (atm)
Q	=	Volumetric rate (cm^3/s)
Subscripts	and	Superscripts
w	=	Related to water phase
n, g	=	Related to gas phase
o	=	Related to oil phase
D	=	Adimensional
$Imb1$	=	1^{st} imbibition cycle
$Drain$	=	1^{st} drainage cycle
$DrainEnd$	=	End point of 1^{st} drainage cycle
$Imb2$	=	2^{nd} imbibition cycle
nm, m	=	Corey equation indices

References

James W. Amyx, Daniel M. Bass, and Robert L. Whiting. *Petroleum Reservoir Engineering: Physical Properties*. McGraw-Hill Book Company, New York, USA, 1960.

E. M. Braun and R. F. Hollan. Relative permeability hysteresis: Laboratory measurements and conceptual model. *SPE Reservoir Engineering*, 1995. SPE 28615.

Patrick Francisco Fuhr Dal'Bó. Análise de carbonatos. Relatório de atividades desenvolvidas, CEPETRO/State University of Campinas, 2012. Convênio da Rede Temática em Capacitação e Tecnologia em Carbonatos (PETROBRAS).

Henry Darcy. Les fontaines publiques de la ville de dijon. *Dalmon, Paris, France*, 1856.

Carlos Roberto Carvalho de Holleben. Determinação de porosidade e saturações de fluidos através de tomografia computadorizada de raios-x. Master's thesis, State University of Campinas, 1993.

Erle C II Donaldson, George V. Chilingarian, and Ten Fu Yen. *Enhanced Oil Recovery: Processes and Operations.* Elsevier Science Publisher B. V., New York, USA, 1989.

D. J. Element, J. H. K. Masters, and N. C. Sarget. Assement of three-phase relative permeability models using laboratory hysteresis data. 2003. SPE 94903.

O. O. Eleri and A. Skauge. Steady-state and unsteady-state two-phase relative permeability hysteresis and measuraments of three-phase relative permeabilities using imaging techniques. 1995. SPE 30764.

Mehdi Honarpour, Leonard Koederitz, and A. Herbert Harvey Snippet. *Relative Permeability of Petroleum Reservoirs*, volume 144. CRC Press Inc., Florida, USA, 2 edition, 1987.

S. J. Hosseini, S. M. M. Mirkalaei, A. Ataei, and Bisol M. R. Investigating the effect of hysteresis modelling on numerical simualtion of imiscible wag injecion. *International Petroleum Technology Conference, Bangkok, Thailand*, February 2012. IPTC-15055-MS.

MadHav M. Kulkarni. Immiscible and miscible gas-oil displacements in porous media. Master's thesis, Louisiana State University, USA, August 2003.

C. S. Land. Comparison of calculated with experimental imbibition relative permeability. *SPEJ*, 11(4):419–425, 1971. SPE 3360-PA.

J. A. Larsen and A. Skauge. Methodology for numerical simulation with cycle-dependent relative permeabilities. *SPEJ*, 3(2): 163–173, 1998. SPE 38456-PA.

Carlos Espinosa Leon and Rosângela Barros Zanoni Lopes Moreno. Wettability characterization of coquina rock from the coqueiro seco formation, sergipe-alagoas basin - brazil. State University of Campinas. Intern communication, 2012.

Leandro Freitas Lopes and Rosângela Barros Zanoni Lopes Moreno. Análise experimental de injeção de polímeros para recuperação de petróleo em carbonatos. State University of Campinas. Intern communication, 2012.

F. Mees, R Swennem, M. Van Geet, and P. Jacobs, editors. *Application of X- Ray Computed Tomography in the Geosciences*, volume 215 of *Special Publications*. Geological Society, 2003.

A. J. Rosa, R. S. Carvalho, and J. A. D. Xavier. *Engenharia de Reservatórios de Petróleo*. Editora Inteciência, Rio de Janeiro, Brazil, 2006.

L. Néstor Sanchez. Management of water alternating gas (wag) injection projects. *Society of Petroleum Engineers*, April 1999. SPE 53714.

J. M. Schembre and A. R. Kovscek. A technique for measuring two-phase relative permeability in porous media via x-ray ct measuraments. *JPT*, 39:159–174, 2003.

E. J. Spiteri. Relative permeability hysteresis: A new model and impact on reservoir simulation. Master's thesis, Stanford University, June 2005.

E. J. Spiteri and R. Juanes. Impact of relative permeability hysteresis on numerical simulation on wag injection. *JPSE*, 50: 115–139, 2006.

M. B. Standing. Notes on relative permeability relantioships. Technical report, The University of Trondhein, August 1974.

S. L. Wellington and H. J. Vinegar. Tomographic imaging of three-phase flow experiments. *Science Instrum.*, 58(1):96–107, January 1987.

E. M. Withjack and J. R. Duham. Relative permeability measurements in carbonate rock.

8 SI Metric Conversion Factors

$cP \times 1.0$	$E^{-03} =$	$Pa.s$
$mD \times 9.869233$	$E^{-04} =$	mm^2
$psi \times 6.894757$	$E^{+00} =$	kPa